coatings

MDPI

Article

In Situ Modulation of Oxygen Vacancy Concentration in $Hf_{0.5}Zr_{0.5}O_{2-x}$ Thin Films and the Mechanism of Its Impact on Ferroelectricity

Shikai Liu [1], Xingyu Li [1], Gang Li [1], Shaoan Yan [1,*], Yingfang Zhu [1,*], Yujie Wu [1], Qin Jiang [1], Yang Zhan [1] and Minghua Tang [2]

[1] School of Mechanical Engineering and Mechanics, Xiangtan University, Xiangtan 411105, China; shikaivv@126.com (S.L.); lxy123202306@163.com (X.L.); ligang@xtu.edu.cn (G.L.); 15580127879@163.com (Y.W.); jiangqin2024@126.com (Q.J.); zhanyang2024@126.com (Y.Z.)

[2] School of Materials Science and Engineering, Xiangtan University, Xiangtan 411105, China; tangminghua@xtu.edu.cn

* Correspondence: yanshaoan@xtu.edu.cn (S.Y.); yfzhu@xtu.edu.cn (Y.Z.)

Abstract: Oxygen vacancies play a crucial role in stabilizing the ferroelectric phase in hafnium (Hf) oxide-based thin films and in shaping the evolution of their ferroelectric properties. In this study, we directly manipulated the oxygen vacancy concentration in $Hf_{0.5}Zr_{0.5}O_{2-x}$ (HZO) ferroelectric thin films in situ using oxygen plasma treatment. We scrutinized the variations in the ferroelectric properties of HZO films across different oxygen vacancy concentrations by integrating the findings from ferroelectric performance tests. Additionally, we elucidated the mechanism underlying the influence of oxygen vacancies on the coercive field and polarization properties of HZO ferroelectric films through the first-principles density functional theory (DFT) calculations. Finally, to study the impact of oxygen vacancies on the practical application of HZO ferroelectric synaptic devices, leveraging the plasticity of the ferroelectric polarization, we constructed a multilayer perceptron (MLP) network. We simulated its recognition accuracy and convergence speed under different oxygen vacancy concentrations in the MNIST recognition task.

Keywords: ferroelectrics; oxygen vacancy; oxygen plasma; DFT calculations; MLP network

Citation: Liu, S.; Li, X.; Li, G.; Yan, S.; Zhu, Y.; Wu, Y.; Jiang, Q.; Zhan, Y.; Tang, M. In Situ Modulation of Oxygen Vacancy Concentration in $Hf_{0.5}Zr_{0.5}O_{2-x}$ Thin Films and the Mechanism of Its Impact on Ferroelectricity. *Coatings* **2024**, *14*, 1121. https://doi.org/10.3390/coatings14091121

Academic Editor: Denis Nazarov

Received: 30 July 2024
Revised: 29 August 2024
Accepted: 30 August 2024
Published: 2 September 2024

1. Introduction

Hafnium oxide (HfO_2) is a material characterized by a wide bandgap and a high dielectric constant, and it was initially employed as a replacement for silicon dioxide gate insulators in CMOS technology. HfO_2 films can transition from the tetragonal phase to the monoclinic phase upon annealing or doping, forming the orthorhombic phase with non-centrosymmetric structures and exhibiting excellent ferroelectric properties [1,2]. Ferroelectric HfO_2 is fully compatible with silicon-based CMOS processes. It can achieve a physical thickness of less than 10 nm, thereby addressing the challenges of size scaling and CMOS process compatibility faced by traditional ferroelectric materials [3]. Hafnium oxide-based ferroelectric films have a simple composition, are easy to control in deposition processes, exhibit large remanent polarization, and possess a wide bandgap, making them highly suitable for memory device applications. Hafnium-based ferroelectric materials exhibit excellent radiation resistance. The memory cells utilize the bistable polarization of the ferroelectric films to store "0" and "1" states. Typically, radiation sources such as heavy ions and gamma rays do not cause complete switching of the polarization state, making it impossible to alter the storage state of ferroelectric memory cells. This property endows hafnium ferroelectric devices with solid radiation resistance [4]. The non-volatility of hafnium-based ferroelectric devices is closely tied to the mechanism of ferroelectric domain switching. Regardless of where the ferroelectric domains switch, the device maintains

a high resistance state externally, inherently possessing low power consumption characteristics [5]. Consequently, hafnium oxide-based ferroelectric materials have garnered significant attention from the academia and industry. Research in this area is anticipated to advance the development and practical application of ferroelectric capacitors, ferroelectric tunnel junctions, ferroelectric transistors, ferroelectric memory, and ferroelectric compute-in-memory technologies [6–11].

The most extensive research on the performance regulation of hafnium oxide-based ferroelectric thin films involves doping methods, with zirconium (Zr)-doped hafnium oxide being the most widely studied and exhibiting the best performance. However, achieving ferroelectric properties through doping introduces defects into the hafnium oxide films, with oxygen vacancies having the most significant impact. Furthermore, the ferroelectricity of hafnium oxide depends on the orthorhombic $Pca2_1$ phase [12,13], which has a higher energy than the monoclinic $P2_1/c$ phase. Consequently, the orthorhombic $Pca2_1$ phase is not stable in its free state. As a result, hafnium oxide-based ferroelectric thin films still face significant challenges in practical applications, such as wake-up effects, fatigue failure, and imprint failure. Zhou et al. [14] discovered that an increase in the concentration of oxygen vacancies decreases the energy difference between the monoclinic and orthorhombic phases, enhancing the stability of the ferroelectric orthorhombic phase. Hoffmann et al. [15] found that oxygen vacancies contribute to a higher proportion of the orthorhombic phase in HfO_2 ferroelectric thin films by reducing the energy difference between the orthorhombic and monoclinic phases.

While previous research has indicated that oxygen vacancies can stabilize ferroelectric phases and enhance residual polarization, it does not imply that more oxygen vacancies are always better. Goh et al. [16] reduced the concentration of oxygen vacancies in HZO films by using RuO_2 electrodes, thereby mitigating the wake-up and fatigue effects. Pešić et al. [17] conducted simulations to study the movement of oxygen vacancies under an electric field. They found that oxygen vacancies are initially concentrated near the electrode interfaces. With a cyclic electric field application, oxygen vacancies gradually diffuse into the interior of the films. These oxygen vacancy-pinned ferroelectric domains can undergo polarization switching, leading to an increase in remanent polarization and the wake-up of the films. During the wake-up process, the diffusion of oxygen vacancies causes the built-in electric field to become more uniform. It is often accompanied by the transformation from the monoclinic phase to the orthorhombic phase. Adkins et al. [18] performed wake-up tests on HZO at different temperatures, ranging from 293 K to 33 K. They observed that the lower the temperature during the wake-up process, the smaller the polarization increase and the more cycles required to achieve full wake-up. This phenomenon is likely due to the reduced mobility of oxygen vacancies at lower temperatures, necessitating more electric field cycles to achieve a more uniform distribution of vacancies within the films. Fengler et al. [19] and Islamov et al. [20,21] observed increased charged defects during the wake-up process in HZO and La-doped HfO_2 films, respectively. They attributed these increased charged defects primarily to oxygen vacancies. Kim et al. [22] employed a novel high-pressure oxygen annealing process on HZO films, resulting in samples with improved wake-up effects compared to those annealed in nitrogen and vacuum environments. Using stable electrodes or those capable of providing additional oxygen to the ferroelectric layer can also reduce oxygen vacancies in the films and mitigate the wake-up effect. Kashir et al. [23] achieved HZO films with almost no wake-up effect by employing W electrodes and optimizing the HZO preparation process. In our previous work, HZO ferroelectric films were prepared using W and Pt as the top and bottom electrodes, respectively. The ferroelectric films with tungsten W electrodes exhibited higher polarization intensity, a flatter fatigue characteristic curve, and a weaker wake-up effect [24].

The movement of oxygen vacancies under an electric field causes wake-up effects and significantly increases the leakage current in the films [25]. The presence of oxygen vacancies introduces trap energy levels into the electronic structure of the system. Electrons do not fully occupy these trap energy levels, allowing external electrons to transition

between them. Numerous traps form an electron pathway when the films contain many oxygen vacancies. Under the influence of an external electric field, this results in significant leakage current in the films, leading to the degradation of ferroelectric performance. Oxygen vacancies significantly impact the stability of the ferroelectric phase in hafnium oxide-based films and play a crucial role in the evolution of ferroelectric properties. Wake-up, imprint, and fatigue effects are all believed to be related to the migration and redistribution of oxygen vacancies under electric field cycling [26–28]. The current research primarily focuses on controlling the number of oxygen vacancies through the preparation process to compare the performance changes in hafnium oxide ferroelectric films and infer the mechanism of oxygen vacancy influence. However, due to the numerous factors affecting the performance of these films, it is challenging to eliminate other variables between different batches of samples. This limitation hinders the judgment and summary of the rules governing the influence of oxygen vacancies on ferroelectricity. Additionally, regulating the oxygen vacancy concentration through the preparation process introduces a degree of randomness, resulting in weak experimental reproducibility and limited reference value. Based on previous reports, oxygen plasma treatment can oxidize non-stoichiometric metal oxide films and form near-stoichiometric metal oxides on the surface [29], i.e., oxygen ions can partially fill oxygen vacancies in HfO_x films after oxygen plasma treatment. As the treatment time increases, there will be a greater chance of filling the oxygen vacancies in the samples. In this work, we directly adjusted the oxygen vacancy concentration in situ in the same batch of HZO ferroelectric films using an oxygen plasma treatment technique, which has the advantage of introducing as few variables as possible. We discussed the variations in the ferroelectric properties of HZO films with different oxygen vacancy concentrations through ferroelectric testing. We analyzed the impact of oxygen vacancies on polarization reversal in HZO ferroelectric films using DFT calculations. Additionally, we discussed how changes in the switching barrier, induced by varying oxygen vacancy concentrations, impact the coercive field of the sample, as revealed by our DFT calculation results. Finally, to study the impact of oxygen vacancies on the practical application of HZO ferroelectric synaptic devices, leveraging the plasticity of the ferroelectric polarization, we constructed an MLP network. We simulated its recognition accuracy and convergence speed under different oxygen vacancy concentrations in the MNIST recognition task.

2. Experimental and Theoretical Methods

A 20 nm W bottom electrode was fabricated using electron beam evaporation on a p-type silicon substrate. The HZO ferroelectric thin films were prepared by atomic layer deposition (PEALD−150R, provided by Jiaxing Kemin Electronic Equipment, Jiaxing, China) using $Hf[N(CH_3)(C_2H_5)]_4$ and $Zr[N(CH_3)(C_2H_5)]_4$ as the precursors for Hf and Zr, respectively. A 10 nm HZO film was deposited on the substrates with the pre-deposited W bottom electrode. On the HZO films, 20 nm thick circular W top electrodes were fabricated using an electron beam evaporation system (TEMD500, provided by Beijing Technol Science, Beijing, China) with a metal mask. The prepared samples underwent rapid thermal annealing at 550 °C in a nitrogen atmosphere for 200 s. The prepared samples were subjected to oxygen plasma treatment (OPT) using an inductively coupled plasma system, (ICP−601, provided by Beijing Chuangshiweina, Beijing, China) with 10 s and 20 s treatment times, respectively. Subsequently, electrical properties and physical phases were characterized on the same device. The polarization (P)-electric field (E) hysteresis loops of the HZO ferroelectric devices were characterized using a ferroelectric analyzer (TFAnalyzer 3000 Basic Unit, provided by aixACCT Systems GmbH, Aachen, Germany). Grazing-incidence X-ray diffraction (GIXRD, Bruker D8, provided by Bruker, Massachusetts, USA) was used to analyze the crystal orientation of the HZO films; the target material used was copper, with an X-ray wavelength of 1.5406 Å, operating at a current of 200 mA and a voltage of 45 kV. We utilized X-ray photoelectron spectroscopy (XPS, Thermo Kalpha, provided by Thermo Fisher Scientific, Massachusetts, USA.) to analyze the chemical states

and oxygen vacancies. We used an Al Kα X-ray source (hv = 1486.6 eV), 12 kV operating voltage, and a 6 mA filament current.

We simulated the polarization–switching process of HZO films with varying oxygen vacancy concentrations using DFT calculations. All DFT calculations were performed using the Vienna Ab initio Simulation Package (VASP) with the Perdew–Burke–Ernzerhof (PBE) type generalized gradient approximation (GGA). The polarization–switching process in $Hf_{0.5}Zr_{0.5}O_2$-based materials was modelled using a periodically repeated $2 \times 2 \times 2$ supercell containing 16 Hf atoms, 16 Zr atoms, and 64 O atoms. This method allows for constructing two models with corresponding atomic positions for upward and downward polarization, which is crucial for applying the climbing-image nudged elastic band (CINEB) method to calculate the energy barrier along the polarization–switching pathway. To simulate polarization–switching under different oxygen vacancy conditions, we constructed two models with varying oxygen vacancy concentrations and considered different polarization directions: 1. removal of one oxygen atom to create an oxygen vacancy concentration of 1.56%; 2. removing two oxygen atoms creates an oxygen vacancy concentration of 3.12%, with these two vacancies positioned as far apart as possible to minimize their interaction effects. Considering the possible configurations of two oxygen vacancies within a $2 \times 2 \times 2$ supercell, there would be a total of $64 \times 63 = 4032$ configurations, which would demand enormous computational resources, given the crystal model's large size. We adopt a common approach to address this by placing the two oxygen vacancies far apart, localizing their influence and minimizing the direct interaction between vacancies. This method better simulates the behavior of isolated defects. It is essential because it likely reflects the actual distribution of oxygen vacancies in a giant crystal, where such vacancies would naturally be dispersed. The switching potential energy curves and energy barriers are calculated using a climbing-image nudged elastic band (CINEB) method to explore the ferroelectric switching process in $Hf_{0.5}Zr_{0.5}O_{2-x}$. We used a $2 \times 2 \times 2$ Monkhorst–Pack k-point mesh for structural optimization and CINEB calculations, terminating the NEB calculations when the root mean square force on the images was less than 0.03 eV/Å.

We fitted the synaptic characteristic curves (plasticity curve of ferroelectric thin films polarization value under voltage) of the samples. We devised an MLP model for MNIST handwritten digit recognition to leverage this synaptic plasticity. Beyond incorporating the concept of ferroelectric polarization-based synaptic plasticity from experimental data into our weight adjustment strategy, we also delved into the relationship between the model's performance before and after OPT. Our MLP architecture is characterized by its first and second hidden layers, comprising 128 and 64 neurons, respectively, with the ReLU activation function applied to both layers. This configuration aims to strike a balance between model complexity and generalization ability. We implemented a callback function to maintain a vigilant eye on the model's learning progress and evaluate its performance. This multifaceted function logs the current model accuracy upon completing each training batch. It conducts a comprehensive accuracy assessment across the entire test set at the end of each training epoch. Furthermore, the callback function updates the model weights after each epoch. This process adheres strictly to the principles of the backpropagation algorithm, adjusting the weight parameters by calculating gradients, thereby guiding the model towards progressively optimal solutions. In this manner, we ensure that every step of the model's training journey is directed towards the right path.

3. Results and Discussion

We characterized the three groups of samples using GIXRD, and the results are depicted in Figure 1. By comparing them with standard PDF cards PDF#34–1084 (orthorhombic phase), PDF#43–1017 (monoclinic phase), PDF#50–1089 (tetragonal phase), and PDF#47–1319 (W), we observed diffraction peaks corresponding to the o phase, t phase, and m phase in all samples, with minimal impurities. This indicates that the prepared samples exhibit ferroelectricity and high purity. The slight shift in the W characteristic peak is likely due to different stresses arising from the varying thicknesses of the W electrodes.

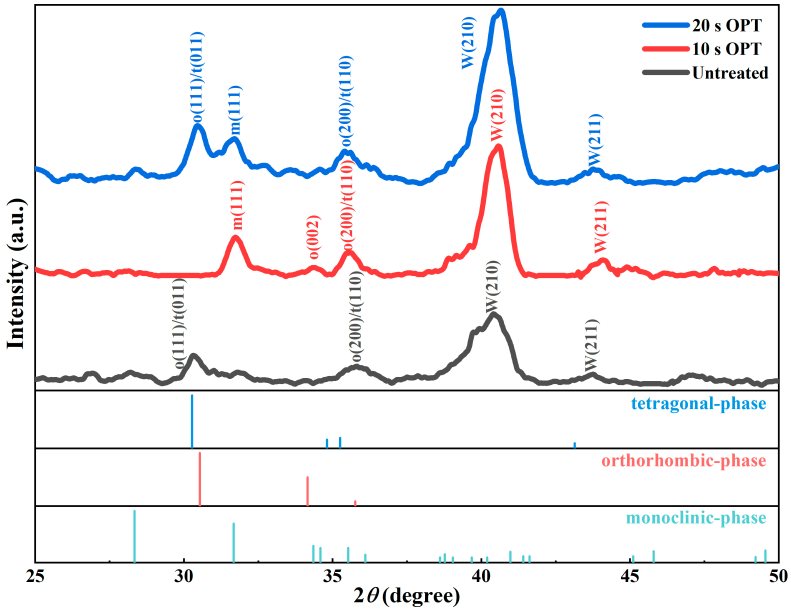

Figure 1. XRD analysis results of samples subjected to varying OPT times.

Figure 2 shows the Hf 4*f* and Zr 3*d* core levels XPS spectra for the samples before and after OPT. As the OPT time increases, the Hf 4*f* and Zr 3*d* peaks shift to higher binding energies. This shift is due to the reduction in oxygen vacancies, which increases the number of electrons taken by oxygen atoms from hafnium and zirconium atoms, thereby raising the binding energies corresponding to these elements [16,30]. By maintaining the ratio of the area of the Hf $4f_{5/2}$ and Hf $4f_{7/2}$ peaks to the total peak area and fitting with Gaussian functions, we identified the contribution corresponding to the Hf^{3+} chemical state. Similarly, we identified the contribution corresponding to the Zr^{3+} chemical state [31,32], as shown by the shaded areas in Figure 2.

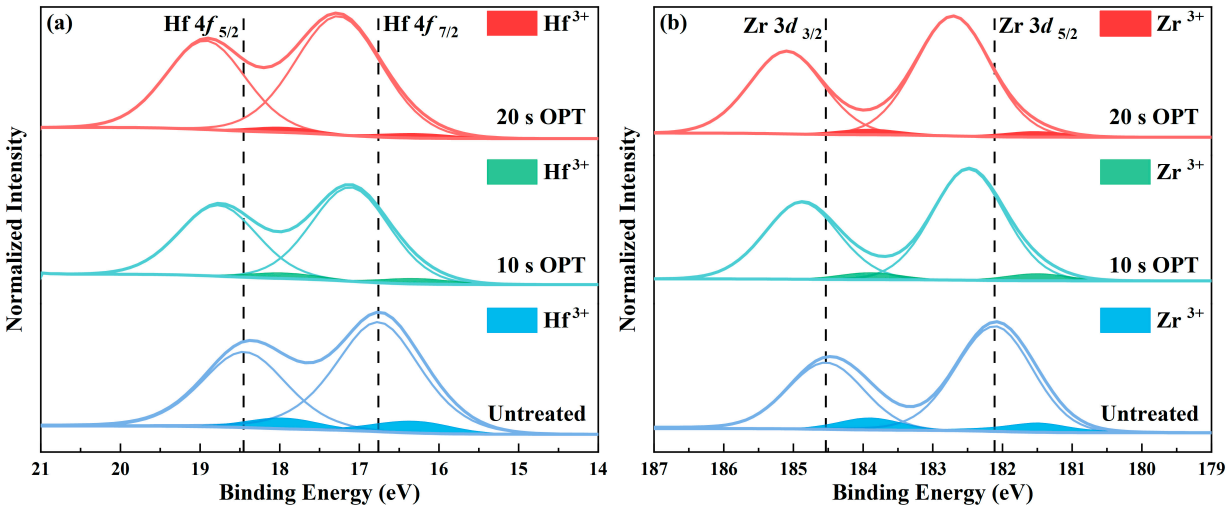

Figure 2. XPS spectra of the samples with different OPT times: (**a**) Hf 4*f* and (**b**) Zr 3*d*.

Oxygen vacancies prevent adjacent metal atoms from forming chemical bonds with oxygen atoms, resulting in a +3 valence state. Therefore, the concentrations of Hf^{3+} and Zr^{3+} can be used to estimate the concentration of oxygen vacancies in the samples [11]. To determine the oxygen vacancy concentration semi-quantitatively, we considered the ratio of the peak areas corresponding to Hf^{3+} and Zr^{3+} to the total peak area as the concentrations of Hf^{3+} and Zr^{3+}. Figure 3a–c show the *P-E* hysteresis loops of the samples under different

applied voltages. As shown in Figure 3d, the oxygen vacancy concentrations of the samples were controlled at 5.07%, 3.02%, and 2.03%, respectively. We found that the oxygen vacancy concentration in the samples significantly decreased after OPT, while extending the treatment time had a limited effect on further reducing oxygen vacancies. As shown in Figure 3e,f, the coercive field and the remanent polarization values of the samples increased with the applied voltage. Notably, within the applied voltage range of 2.5 V to 4 V, the changes in the coercive field for the samples before and after OPT were 0.2 MV/cm, 0.29 MV/cm, and 0.38 MV/cm, respectively, while the changes in remanent polarization were 5.8 μC/cm^2, 6.44 μC/cm^2, and 12.61 μC/cm^2. The samples without OPT exhibited the most significant changes in coercive field and remanent polarization, whereas the samples treated with plasma for 20 s had the most minor differences. This indicates that a moderate increase in oxygen vacancy concentration can modulate the samples to achieve more remanent polarization states, offering better multilevel control capabilities. The HZO ferroelectric films we fabricated are wake-up free, as demonstrated in Figure 4a, primarily due to implementing a unidirectional annealing process [33]. We also presented the fatigue characteristics of the ferroelectric films before and after OPT, finding no significant changes in their fatigue properties, as shown in Figure 4b. To better illustrate that ferroelectric devices can be used for in-memory computing neural network operations, we included experimental data on their retention characteristics, demonstrating their non-volatility. In Figure 4c–e, the remanent polarization of the hafnium oxide-based ferroelectric devices is well maintained over time. The effect of oxygen vacancies on HfO_2-based ferroelectric films is complex. In this study, we focused on the impact and mechanism of oxygen vacancies on the coercive field of HZO ferroelectric films, as the coercive field directly influences the multilevel characteristics of HZO films, which in turn affects their application in computing-in-memory systems.

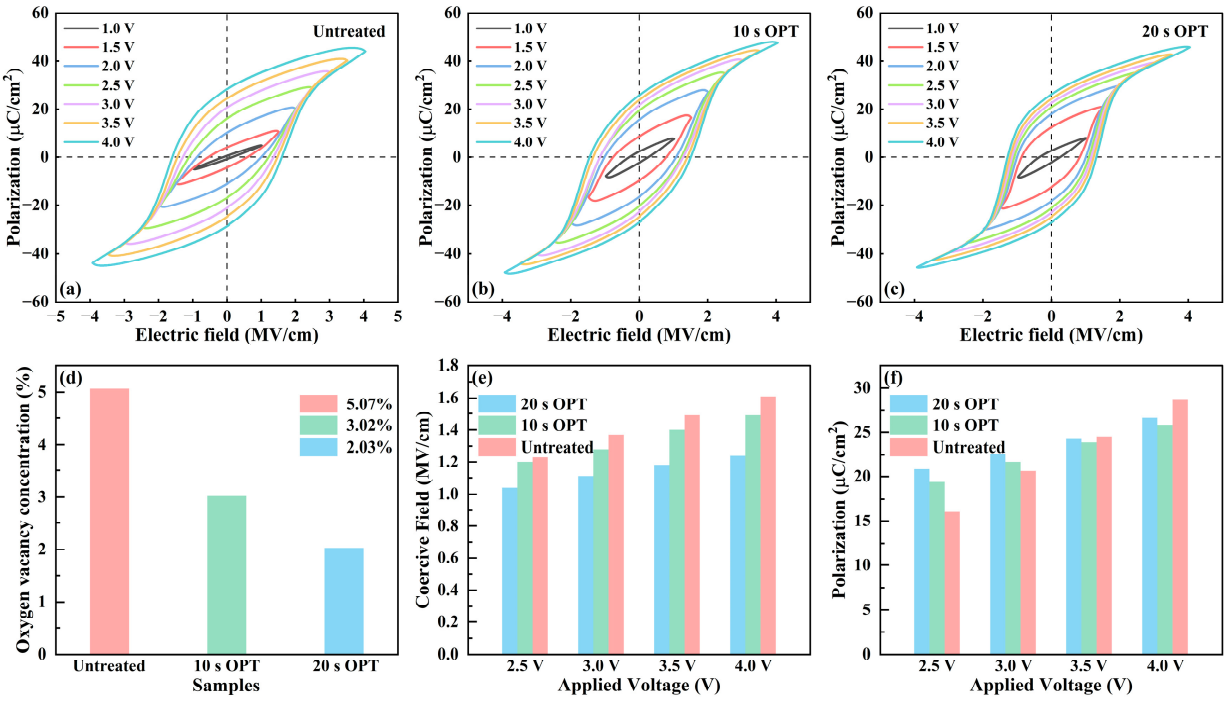

Figure 3. (**a**) *P-E* hysteresis loops of samples that are untreated, (**b**) with 10 s OPT, and (**c**) with 20 s OPT. (**d**) Oxygen vacancy concentrations of samples with different OPT times. (**e**) Coercive field values and (**f**) remanent polarization values of the samples under different applied voltages.

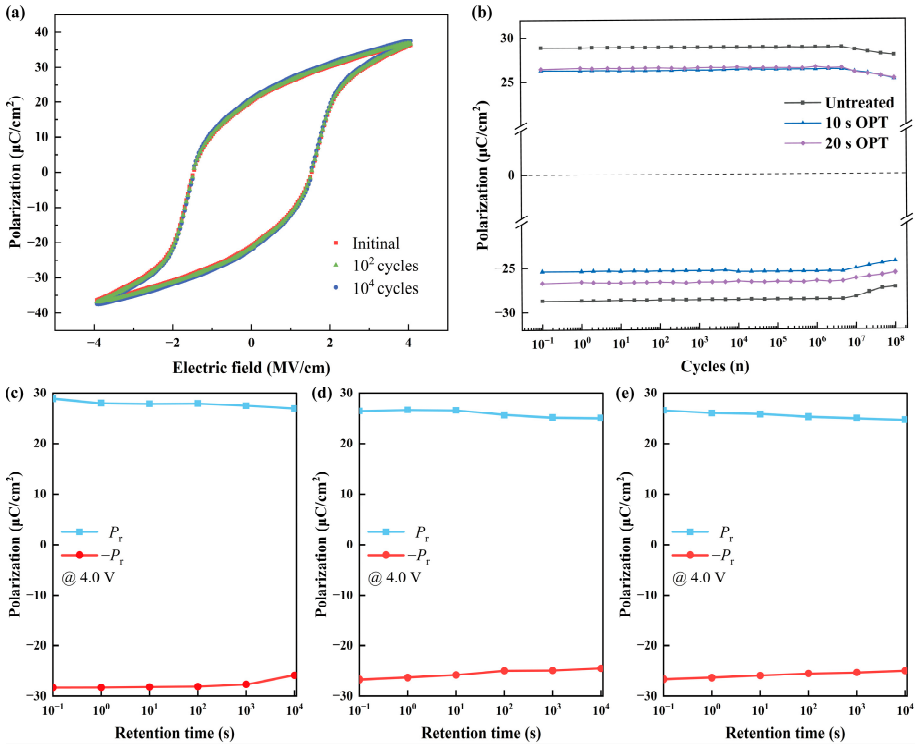

Figure 4. (**a**) The retention and (**b**)fatigue characteristics curve of the samples. (**c**) Retention characteristic curve of samples that are untreated, (**d**) with 10 s OPT, and (**e**) with 20 s OPT.

We used DFT calculations to explain the effects of oxygen vacancies on the coercive field and multilevel polarization characteristics of HZO ferroelectric thin films. Figure 5 illustrates the energy states of HZO films with oxygen vacancy concentrations of 1.56% and 3.13% under three polarization states. We found that increasing the oxygen vacancy concentration raises the energy of the intermediate state, thereby increasing the switching barrier. This is likely because more oxygen vacancies must migrate during the polarization–switching process. The increase in the switching barrier leads to a larger coercive field, allowing for the modulation of more intermediate coercive field values. Consequently, more remanent polarization states are obtained, resulting in better multilevel characteristics of the device [34].

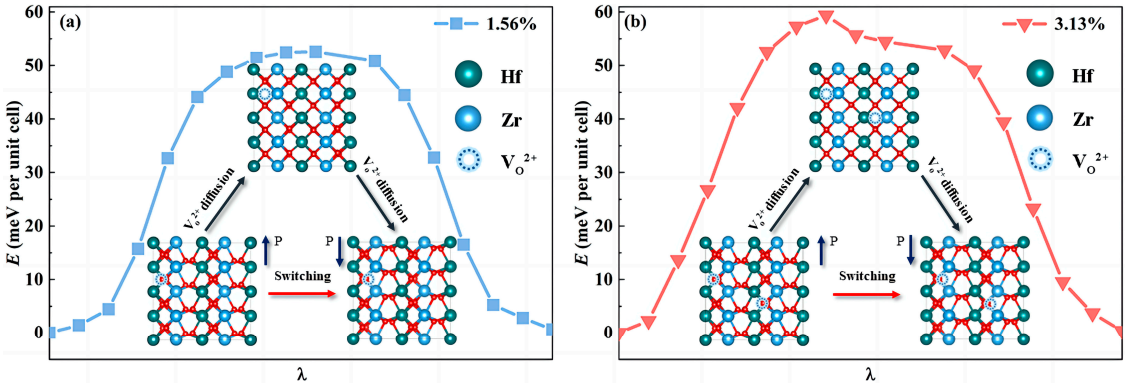

Figure 5. Energy profiles for polarization–switching and switching paths in the 2 × 2 × 2 supercell model of $Hf_{0.5}Zr_{0.5}O_{2-x}$, with oxygen vacancy concentrations of (**a**) 1.56% and (**b**) 3.13%.

In applications related to biological synapses, the acceptable remanent polarization value of ferroelectric materials is determined by the readout precision of peripheral circuits and energy efficiency requirements. Higher readout precision in peripheral circuits

allows for a smaller acceptable remanent polarization value. Although a smaller remanent polarization value reduces the device's energy consumption, it can also increase the energy required by the peripheral circuits during readout. It is well known that the remanent polarization of hafnium oxide-based ferroelectric films is nonvolatile and can achieve different remanent polarizations under various applied voltages. This plasticity of polarization is highly analogous to the characteristics of biological synapses, laying a foundation for its ability to perform neural network computations based on the in-memory computing architecture (Figure 6a). In the architecture of neural network computations, the multiply-accumulate (MAC) operation holds a pivotal position. It is explicitly tasked with efficiently performing the multiplication of the input vector by the weight matrix within the framework of each layer of network connections. This serves as the cornerstone for driving the data processing and learning capabilities of neural networks. The mathematical form of this process is the following:

$$(y_1, y_2, \cdots, y_m)^T = W_{m\times n} \times (x_1, x_2, \cdots, x_n)^T \quad (1)$$

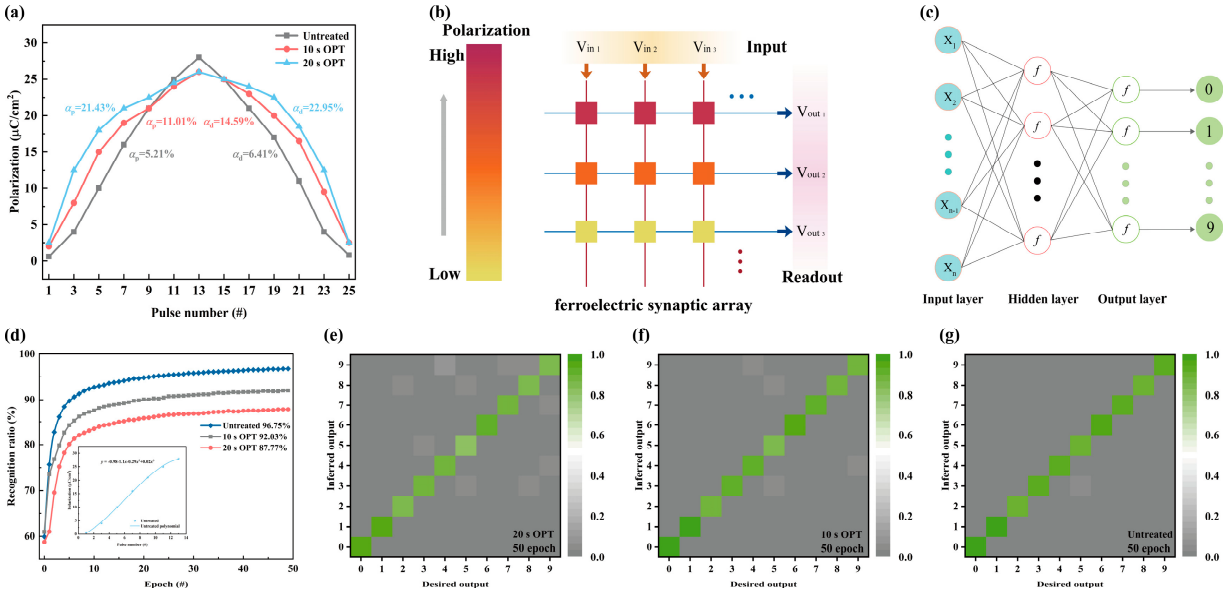

Figure 6. (**a**) Synaptic characteristic curves of samples that are untreated, samples with 10 s OPT, and samples with 20 s OPT; (**b**) the crossbar array of the synaptic devices; (**c**) the MLP network connections; (**d**) recognition accuracy curve of samples that are untreated, samples with 10 s OPT, and samples with 20 s OPT; (**e**–**g**) average confusion matrix of samples that are untreated, samples with 10 s OPT, and samples with 20 s OPT.

In the crossbar array architecture depicted in Figure 6b, each node represents a ferroelectric synaptic device, each of which possesses the capability of non-volatile weight storage, enabling the retention of weight information even when the power is off. By applying Equation (2), when input signals are encoded in the form of voltages (corresponding to the rows of the array), the corresponding output signals (corresponding to the columns of the array) can be computed. This process fully realizes a MAC operation by incorporating weight values, mapping input data directly to output, significantly facilitating the efficient execution of numerous matrix operations in neural networks, as each layer of the crossbar array directly corresponds to a layer of neural network connections. We selected synaptic plasticity curves influenced by varying oxygen vacancy concentrations to mimic genuine biological synaptic plasticity. We fitted them to accurately reflect the impact of this plasticity

on the weight updates of neural network nodes. Based on this model, we constructed an MLP for handwritten digit recognition, as illustrated in Figure 6c.

$$V_{out_j} = \frac{\sum_{i=1}^{\text{Input}} P_{ij,Fe} V_{in_i}}{P_{reference}} \quad (2)$$

Figure 6a illustrates the polarization plasticity of three sets of ferroelectric synaptic devices. When a continuous positive voltage is applied to the device, its remanent polarization increases. Conversely, the remanent polarization decreases with increasing negative voltage applications. The nonlinearity of the curves ($\alpha p/\alpha d$) was determined by performing least-squares fitting on synaptic plasticity curves. The comparison shows that the sample without oxygen plasma treatment exhibits the lowest nonlinearity, at 5.21%/6.41%. After applying continuous pulses, we aspire to achieve linearly modulated polarization states with a diverse range of stable polarization states. To train the MLP network, we utilized a handwritten digit dataset consisting of 60,000 training images and 10,000 testing images. By setting the learning rate rationally, we successfully prevented overfitting while ensuring model convergence. To ensure the stability and reliability of the MLP model, we set the learning rate to 0.003 and calculated both the training and test accuracies. This learning rate guarantees model convergence and effectively mitigates the risk of overfitting. Upon examining the trends presented in Figure 6d, it becomes evident that during the initial stages of training with untreated samples, the recognition accuracy of the MLP model rapidly soars. As the training iterations accumulate, reaching a milestone of 50, the recognition accuracy attains an impressive 96.75%. Zhu et al. [35] investigated $HfZrO_x$-based ferroelectric synaptic devices and applied them to MNIST recognition tasks, achieving a pattern recognition accuracy of 93.38%. Furthermore, Zhang et al. [36] fabricated ferroelectric synaptic devices that achieved recognition accuracy of 90.3% in MNIST recognition tasks. In comparison, the synaptic devices we developed demonstrated superior performance. The MLP model we used is a classic neural network architecture, with no specific modifications made to the network connections, despite using ferroelectric synaptic devices. We consider the plasticity of the remanent polarization in these ferroelectric devices to be the primary factor influencing the weight update process. Consequently, the robustness of the constructed MLP network largely depends on the linearity of the plasticity in the ferroelectric synaptic devices. The higher the linearity, the greater the accuracy and robustness of the MLP network. Due to the poorer linearity of the plasticity curve of the samples after OPT, the weight update process based on their fitted curves is less ideal, resulting in a decrease in accuracy. The average confusion matrices representing recognition accuracy at various training iterations are depicted in Figure 6e–g. As the number of training iterations increases, it becomes evident that the accuracy of recognizing the input digit gradually improves while the probability of misclassifying the remaining digits decreases. Similar to the accuracy curve, the average confusion matrix accuracy of the untreated samples is higher than that of the OPT-treated samples. This matrix demonstrates that the model achieves high recognition accuracy for all digits from 0 to 9. Thus, hafnium-based ferroelectric synaptic devices exhibit substantial potential for hardware-level applications in artificial neural networks; oxygen vacancies significantly impact the neural network application of hafnium-based ferroelectrics due to their influence on the plasticity curve.

4. Conclusions

In this study, we regulated the oxygen vacancy concentrations in situ by adjusting the oxygen plasma treatment time. Within the applied voltage range of 2.5 V to 4 V, as the oxygen vacancy concentration in the samples decreased from 5.07% to 2.03%, the change in coercive field values decreased from 0.38 MV/cm to 0.2 MV/cm. The change in the remanent polarization values decreased from 12.61 $\mu C/cm^2$ to 5.8 $\mu C/cm^2$. The

increase in the oxygen vacancy concentration endows the device with better multilevel control characteristics. The DFT calculations revealed that increasing the oxygen vacancy concentration raises the polarization–switching barriers in the samples, resulting in larger coercive fields under the same applied voltage. Thus, changing the applied voltage can modulate more coercive field values and remanent polarization states. To study the impact of oxygen vacancies on the practical application of HZO ferroelectric synaptic devices, leveraging the plasticity of ferroelectric polarization, we constructed an MLP network. We simulated its recognition accuracy and convergence speed under different oxygen vacancy concentrations in the MNIST recognition task. Using the synaptic characteristic curves of untreated samples, the MLP model achieved a handwritten digit recognition accuracy of 96.75% after 50 training iterations. This indicates that hafnium-based ferroelectric synaptic devices exhibit substantial potential for hardware-level applications in artificial neural networks. Oxygen vacancies can have a significant impact on the neural network application of hafnium-based ferroelectrics due to their influence on the plasticity curve.

Author Contributions: S.L.: investigation, methodology, formal analysis. X.L.: investigation, validation. G.L.: investigation, resources. S.Y.: conceptualization, methodology, investigation, writing—original draft, funding acquisition. Y.Z. (Yingfang Zhu): writing—review and editing, funding acquisition. Y.W.: formal analysis. Q.J.: validation. Y.Z. (Yang Zhan): validation. M.T.: supervision, project administration, funding acquisition. All authors have read and agreed to the published version of the manuscript.

Funding: This work was financially supported by the National Natural Science Foundation of China (Grant Nos. 92164108, U23A20322, 62104267), the Provincial Natural Science Foundation of Hunan (Grant Nos. 2023JJ30599, 2023JJ50009), and the National Key Research and Development Program of China (2023YFF0719600, 2021YFB4000800).

Institutional Review Board Statement: Not applicable.

Informed Consent Statement: Not applicable.

Data Availability Statement: Data are contained within the article.

Conflicts of Interest: The authors declare no conflicts of interest.

References

1. Böscke, T.S.; Müller, J.; Bräuhaus, D.; Schröder, U.; Böttger, U. Ferroelectricity in Hafnium Oxide Thin Films. *Appl. Phys. Lett.* **2011**, *99*, 102903. [CrossRef]
2. Müller, J.; Böscke, T.S.; Bräuhaus, D.; Schröder, U.; Böttger, U.; Sundqvist, J.; Kücher, P.; Mikolajick, T.; Frey, L. Ferroelectric $Zr_{0.5}Hf_{0.5}O_2$ Thin Films for Nonvolatile Memory Applications. *Appl. Phys. Lett.* **2011**, *99*, 112901. [CrossRef]
3. Yan, S.; Zang, J.; Xu, P.; Zhu, Y.; Li, G.; Chen, Q.; Chen, Z.; Zhang, Y.; Tang, M.; Zheng, X. Recent Progress in Ferroelectric Synapses and Their Applications. *Sci. China Mater.* **2023**, *66*, 877–894. [CrossRef]
4. Yan, S.; Zang, J.; Zhu, Y.; Li, G.; Xu, P.; Chen, Z.; Liu, S.; Tang, M. Influence of Metal Electrodes on the Irradiation Resistance of HZO Ferroelectric Thin Film Capacitors and Mechanism Analysis. *J. Alloys Compd.* **2024**, *976*, 173175. [CrossRef]
5. Li, G.; Liu, Y.; Yan, S.; Ma, N.; Xiao, Y.; Tang, M.; Long, Z. Charge-Compensated Co-Doping Stabilizes Robust Hafnium Oxide Ferroelectricity. *J. Mater. Chem. C* **2024**, *12*, 6257–6266. [CrossRef]
6. Oh, S.; Kim, T.; Kwak, M.; Song, J.; Woo, J.; Jeon, S.; Yoo, I.K.; Hwang, H. $HfZrO_x$-Based Ferroelectric Synapse Device with 32 Levels of Conductance States for Neuromorphic Applications. *IEEE Electron Device Lett.* **2017**, *38*, 732–735. [CrossRef]
7. Luo, J.; Xu, W.; Du, Y.; Fu, B.; Song, J.; Fu, Z.; Yang, M.; Li, Y.; Ye, L.; Huang, Q.; et al. Energy- and Area-Efficient Fe-FinFET-Based Time-Domain Mixed-Signal Computing In Memory for Edge Machine Learning. In Proceedings of the 2021 IEEE International Electron Devices Meeting (IEDM), San Francisco, CA, USA, 11–15 December 2021; IEEE: Piscataway, NJ, USA, 2021; pp. 19.5.1–19.5.4.
8. Chen, C.; Yang, M.; Liu, S.; Liu, T.; Zhu, K.; Zhao, Y.; Wang, H.; Huang, Q.; Huang, R. Bio-Inspired Neurons Based on Novel Leaky-FeFET with Ultra-Low Hardware Cost and Advanced Functionality for All-Ferroelectric Neural Network. In Proceedings of the 2019 Symposium on VLSI Technology, Kyoto, Japan, 9–14 June 2019; IEEE: Piscataway, NJ, USA, 2019; pp. T136–T137.
9. De, S.; Muller, F.; Laleni, N.; Lederer, M.; Raffel, Y.; Mojumder, S.; Vardar, A.; Abdulazhanov, S.; Ali, T.; Dunkel, S.; et al. Demonstration of Multiply-Accumulate Operation with 28 Nm FeFET Crossbar Array. *IEEE Electron Device Lett.* **2022**, *43*, 2081–2084. [CrossRef]

10. Soliman, T.; Chatterjee, S.; Laleni, N.; Müller, F.; Kirchner, T.; Wehn, N.; Kämpfe, T.; Chauhan, Y.S.; Amrouch, H. First Demonstration of In-Memory Computing Crossbar Using Multi-Level Cell FeFET. *Nat. Commun.* **2023**, *14*, 6348. [CrossRef]
11. Bao, K.; Liao, J.; Yan, F.; Jia, S.; Zeng, B.; Yang, Q.; Liao, M.; Zhou, Y. Enhanced Endurance and Imprint Properties in $Hf_{0.5}Zr_{0.5}O_{2-\delta}$ Ferroelectric Capacitors by Tailoring the Oxygen Vacancy. *ACS Appl. Electron. Mater.* **2023**, *5*, 4615–4623. [CrossRef]
12. Sang, X.; Grimley, E.D.; Schenk, T.; Schroeder, U.; LeBeau, J.M. On the Structural Origins of Ferroelectricity in HfO_2 Thin Films. *Appl. Phys. Lett.* **2015**, *106*, 162905. [CrossRef]
13. Huan, T.D.; Sharma, V.; Rossetti, G.A.; Ramprasad, R. Pathways towards Ferroelectricity in Hafnia. *Phys. Rev. B* **2014**, *90*, 64111. [CrossRef]
14. Zhou, Y.; Zhang, Y.K.; Yang, Q.; Jiang, J.; Fan, P.; Liao, M.; Zhou, Y.C. The Effects of Oxygen Vacancies on Ferroelectric Phase Transition of HfO_2-Based Thin Film from First-Principle. *Comput. Mater. Sci* **2019**, *167*, 143–150. [CrossRef]
15. Hoffmann, M.; Schroeder, U.; Schenk, T.; Shimizu, T.; Funakubo, H.; Sakata, O.; Pohl, D.; Drescher, M.; Adelmann, C.; Materlik, R.; et al. Stabilizing the Ferroelectric Phase in Doped Hafnium Oxide. *J. Appl. Phys.* **2015**, *118*, 72006. [CrossRef]
16. Shen, Y.; Liang, L.; Zhang, S.; Huang, D.; Zhang, J.; Xu, S.; Liang, C.; Xu, W. Organelle-Targeting Surface-Enhanced Raman Scattering (SERS) Nanosensors for Subcellular pH Sensing. *Nanoscale* **2018**, *10*, 1622–1630. [CrossRef] [PubMed]
17. Pešić, M.; Fengler, F.P.G.; Larcher, L.; Padovani, A.; Schenk, T.; Grimley, E.D.; Sang, X.; LeBeau, J.M.; Slesazeck, S.; Schroeder, U.; et al. Physical Mechanisms behind the Field-cycling Behavior of HfO_2-based Ferroelectric Capacitors. *Adv. Funct. Mater.* **2016**, *26*, 4601–4612. [CrossRef]
18. Adkins, J.W.; Fina, I.; Sánchez, F.; Bakaul, S.R.; Abiade, J.T. Thermal Evolution of Ferroelectric Behavior in Epitaxial $Hf_{0.5}Zr_{0.5}O_2$. *Appl. Phys. Lett.* **2020**, *117*, 142902. [CrossRef]
19. Fengler, F.P.G.; Nigon, R.; Muralt, P.; Grimley, E.D.; Sang, X.; Sessi, V.; Hentschel, R.; LeBeau, J.M.; Mikolajick, T.; Schroeder, U. Analysis of Performance Instabilities of Hafnia-based Ferroelectrics Using Modulus Spectroscopy and Thermally Stimulated Depolarization Currents. *Adv. Electron. Mater.* **2018**, *4*, 1700547. [CrossRef]
20. Islamov, D.R.; Gritsenko, V.A.; Perevalov, T.V.; Pustovarov, V.A.; Orlov, O.M.; Chernikova, A.G.; Markeev, A.M.; Slesazeck, S.; Schroeder, U.; Mikolajick, T.; et al. Identification of the Nature of Traps Involved in the Field Cycling of $Hf_{0.5}Zr_{0.5}O_2$-Based Ferroelectric Thin Films. *Acta Mater.* **2019**, *166*, 47–55. [CrossRef]
21. Islamov, D.R.; Zalyalov, T.M.; Orlov, O.M.; Gritsenko, V.A.; Krasnikov, G.Y. Impact of Oxygen Vacancy on the Ferroelectric Properties of Lanthanum-Doped Hafnium Oxide. *Appl. Phys. Lett.* **2020**, *117*, 162901. [CrossRef]
22. Kim, H.; Kashir, A.; Oh, S.; Jang, H.; Hwang, H. Effects of High Pressure Oxygen Annealing on $Hf_{0.5}Zr_{0.5}O_2$ Ferroelectric Device. *Proc. Spie.* **2021**, *32*, 315712. [CrossRef]
23. Kashir, A.; Kim, H.; Oh, S.; Hwang, H. Large Remnant Polarization in a Wake-up Free $Hf_{0.5}Zr_{0.5}O_2$ Ferroelectric Film through Bulk and Interface Engineering. *ACS Appl. Electron. Mater.* **2021**, *3*, 629–638. [CrossRef]
24. Xu, P.; Yan, S.; Zhu, Y.; Zang, J.; Luo, P.; Li, G.; Yang, Q.; Chen, Z.; Zhang, W.; Zheng, X.; et al. Effects of Different Metal Electrodes on the Ferroelectric Properties of HZO Thin Films. *J. Mater. Sci.-Mater. Electron.* **2023**, *34*, 1915. [CrossRef]
25. Starschich, S.; Menzel, S.; Böttger, U. Pulse Wake-up and Breakdown Investigation of Ferroelectric Yttrium Doped HfO_2. *J. Appl. Phys.* **2017**, *121*, 154102. [CrossRef]
26. Park, M.H.; Kim, H.J.; Kim, Y.J.; Moon, T.; Kim, K.D.; Lee, Y.H.; Hyun, S.D.; Hwang, C.S. Study on the Internal Field and Conduction Mechanism of Atomic Layer Deposited Ferroelectric $Hf_{0.5}Zr_{0.5}O_2$ Thin Films. *J. Mater. Chem. C* **2015**, *3*, 6291–6300. [CrossRef]
27. Mueller, S.; Muller, J.; Schroeder, U.; Mikolajick, T. Reliability Characteristics of Ferroelectric Si:HfO_2 Thin Films for Memory Applications. *IEEE Trans. Device Mater. Reliab.* **2013**, *13*, 93–97. [CrossRef]
28. Glinchuk, M.D.; Morozovska, A.N.; Lukowiak, A.; Stręk, W.; Silibin, M.V.; Karpinsky, D.V.; Kim, Y.; Kalinin, S.V. Possible Electrochemical Origin of Ferroelectricity in HfO_2 Thin Films. *J. Alloys Compd.* **2020**, *830*, 153628. [CrossRef]
29. Lee, M.J.; Lee, C.B.; Lee, D.; Lee, S.R.; Chang, M.; Hur, J.H.; Kim, Y.B.; Kim, C.J.; Seo, D.H.; Seo, S.; et al. A fast, high-endurance and scalable non-volatile memory device made from asymmetric Ta_2O_{5-x}/TaO_{2-x} bilayer structures. *Nat. Mater.* **2011**, *10*, 625–630. [CrossRef]
30. Cho, D.-Y.; Oh, S.-J.; Chang, Y.J.; Noh, T.W.; Jung, R.; Lee, J.-C. Role of Oxygen Vacancy in $HfO_2/SiO_2/Si(100)$ Interfaces. *Appl. Phys. Lett.* **2006**, *88*, 193502. [CrossRef]
31. Baumgarten, L.; Szyjka, T.; Mittmann, T.; Materano, M.; Matveyev, Y.; Schlueter, C.; Mikolajick, T.; Schroeder, U.; Müller, M. Impact of Vacancies and Impurities on Ferroelectricity in PVD- and ALD-Grown HfO_2 Films. *Appl. Phys. Lett.* **2021**, *118*, 32903. [CrossRef]
32. Hamouda, W.; Pancotti, A.; Lubin, C.; Tortech, L.; Richter, C.; Mikolajick, T.; Schroeder, U.; Barrett, N. Physical Chemistry of the $TiN/Hf_{0.5}Zr_{0.5}O_2$ Interface. *J. Appl. Phys.* **2020**, *127*, 64105. [CrossRef]
33. Bai, N.; Xue, K.; Huang, J.; Yuan, J.; Wang, W.; Mao, G.; Zou, L.; Yang, S.; Lu, H.; Sun, H.; et al. Designing Wake-up Free Ferroelectric Capacitors Based on the HfO_2/ZrO_2 Superlattice Structure. *Adv. Electron. Mater.* **2023**, *9*, 2200737. [CrossRef]
34. Zhou, C.; Ma, L.; Feng, Y.; Kuo, C.-Y.; Ku, Y.-C.; Liu, C.-E.; Cheng, X.; Li, J.; Si, Y.; Huang, H.; et al. Enhanced Polarization Switching Characteristics of HfO_2 Ultrathin Films via Acceptor-Donor Co-Doping. *Nat. Commun.* **2024**, *15*, 2893. [CrossRef]

35. Zhu, Y.; He, Y.; Chen, C.; Zhu, L.; Mao, H.; Zhu, Y.; Wang, X.; Yang, Y.; Wan, C.; Wan, Q. $HfZrO_x$-Based Capacitive Synapses with Highly Linear and Symmetric Multilevel Characteristics for Neuromorphic Computing. *Appl. Phys. Lett.* **2022**, *120*, 113504. [CrossRef]
36. Zhang, P.; Ma, X.; Dong, Y.; Wu, Z.; Chen, D.; Cui, T.; Liu, J.; Liu, G.; Li, X. An Energy Efficient Reservoir Computing System Based on HZO Memcapacitive Devices. *Appl. Phys. Lett.* **2023**, *123*, 122104. [CrossRef]